Highly Ordered Polymer Films of Amphiphilic, Regioregular Polythiophene Derivatives

J. Mattu, T. Johansson, S. Holdcroft, and G. W. Leach*

Department of Chemistry, Simon Fraser University, 8888 University Drive, Burnaby, British Columbia V5A 1S6, Canada

Received: December 16, 2005; In Final Form: May 12, 2006

The fabrication and characterization of highly ordered thin films made from amphiphilic, regioregular polythiophene derivatives are described. Films of poly(3-(11-(2-tetrahydropyranyloxy)undecyl)thiophene (PTHPUDT) were prepared by the Langmuir−Blodgett technique. The amphiphilic nature of the polymer affords layer-by-layer deposition and the formation of multilayer films of head-to-head and tail-to-tail Y-type structure. X-ray diffraction studies indicate bilayer separations of ∼30 Å. Anisotropic optical absorption in the plane of the film indicates that the thiophene backbones are preferentially oriented along the dipping direction. Further, polarized light microscopy studies indicate that these films are highly birefringent and that the optical retardation is uniform over the entire film. Ellipsometry studies confirm the sizable magnitude of the birefringence. Optical second-harmonic generation studies of multilayer films provide information regarding both the thiophene orientation within the film and the anisotropic distribution of chromophores in the surface plane. Taken together, these data offer strong evidence of highly ordered films in which the hydrophobic polythiophene chains lie parallel to the substrate surface with their alkyl chains oriented normal to the surface, as dictated by the hydrophilic nature of the alkyl chain's terminal tetrahydropyran functional group. As such, these films offer the potential for elucidating the connection between polymer morphology and physical property in materials that are otherwise subject to a sufficiently complex distribution of morphologies that such a correspondence is precluded.

Introduction

Conjugated polymers have found increasing use as the active media in emerging technologies such as organic light-emitting diodes[1] (OLEDs) and displays, as well as organic field effect transistors[2] (FETs). Because of their unique electrical, optical, and luminescent properties, π-conjugated polymers (πCPs) have been incorporated as photoactive and electroactive layers in these devices. Combined with their ease of processability and relative low cost, these properties make them attractive candidates for long-term replacement of existing technologies and for new niche applications.

With this great potential has come considerable effort to understand and control the physical properties of these polymer systems. The extent of molecular organization in these polymer systems has been shown to be vital in determining their luminescent[3] and conducting[4] abilities and hence their efficacy as device materials. Efforts to control the level of organization have included the development of synthetic strategies for regiochemical control that provide head-to-tail (HT) couplings of monomer units and afford low-energy planar conformations, greater conjugation lengths, and enhanced conductivities. Regioregular (RR) polymers are able to pack with a higher degree of crystallinity in the solid state than do their regioirregular (RIR) analogues, giving rise to smaller band gaps and higher carrier mobilities.[3,4] Importantly, it has also been demonstrated that the structure and orientation of the crystalline domains formed in spin-cast films of poly(3-hexylthiophene) have a dramatic influence on their charge carrier mobilities.[5] Nevertheless, conventional solution casting techniques of these polymers lead to the formation of distributions of crystalline domains with varying properties, depending on the extent of crystallinity, the packing within the domains, the relative domain orientations, as well as the complex morphologies inherent to noncrystalline regions. As a result, the detailed structural properties of πCP-based thin films have remained difficult to characterize and control. Attempts to unravel the connection between polymer conformation and physical property in systems of complex morphology represent a significant challenge and an area of active investigation.

One potentially useful strategy to impart morphological control over large areas is the use of external forces to control molecular order. Kim and Swager have used this strategy to examine the intrinsic spectroscopic properties of poly(*p*-phenylene-ethynylene) Langmuir films by varying chain conformation and interpolymer interactions through changes in mechanical force.[6] Specific tailoring of functional group properties to synthesize amphiphilic polymers that preferentially order at the water/air interface has also been examined. The degree of molecular order in these films is due not only to intermolecular interactions within the film (as for spin-cast or drop-cast films) but also from those forces inherent to the interface and from those under external (mechanical) control. The introduction of polar functionalities into polyalkylthiophenes in the proximity of the thiophene chain[7,8] or in the pendant alkyl groups[9,10] has permitted the fabrication of LB structures of various architectures, without the requirement for dilution with other amphiphiles. Likewise, the characterization of Langmuir films of amphiphilic, bithiophene-based RR polymers have shown that they form large, highly ordered domains, distinct from the dramatically lower degree of crystallinity evidenced in less regioregularly coupled polymers.[11]

* To whom correspondence should be addressed. E-mail: gleach@sfu.ca. Telephone: (604)291-5493. Fax: (604)291-3765.

10.1021/jp057346m CCC: $33.50
Published on Web 07/19/2006

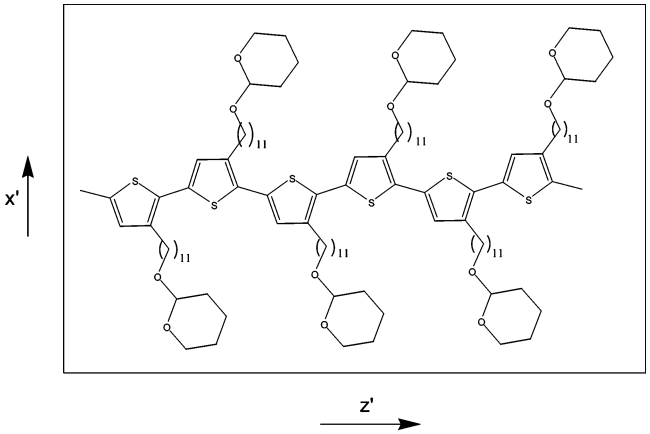

Figure 1. Structure of poly(3-(11-(2-tetrahydropyranyloxy)undecyl)-thiophene (PTHPUDT).

One important example of a πCP with attractive properties is poly(3-(2-(2-tetrahydropyranyloxy)ethyl)thiophene) (PTHPET), which has potential lithographic applications due to its ability to be patterned with micron resolution via chemically amplified photolithography[12] (CAP). In this process, the tetrahydropyranyl (THP) group is photochemically converted to a hydroxyl group by acid catalysis, changing the polymer's solubility. Here, we describe studies on a more soluble analogue of this polymer, poly(3-(11-(2-tetrahydropyranyloxy)undecyl)-thiophene) (PTHPUDT) shown in Figure 1. This polymer is composed of a hydrophobic polythiophene chain with hydrophilic THP groups that terminate the pendant alkyl chains. Here, we show that well-ordered monolayers of PTHPUDT can be formed at the air/water interface and these layers can be deposited into highly ordered multilayer films by the Langmuir−Blodgett technique. Further, these films display significantly red-shifted absorption features consistent with planar conformation and a high degree of conjugation. These films offer the possibility of examining the detailed chemistry responsible for photodeprotection and lithographic pattern formation in well-ordered and highly structured environments.

To help characterize the extent of ordering upon processing these polymers into thin films, we have conducted absorbance, surface wettability, optical microscopy, X-ray diffraction (XRD), atomic force microscopy (AFM), transmission electron microscopy (TEM), and nonlinear optical second-harmonic generation (SHG) measurements of PTHPUDT films deposited onto solid substrates. In what follows, we describe the method of film deposition and the experimental apparatus used to carry out these studies. Following this, we present the results of our characterization studies, including a surface SHG analysis, which shows that there exists well-defined order in the films and allows us to confirm the orientation of the polymer within the film.

Experimental Section

The synthesis of PTHPUDT has been discussed in detail previously.[12] Briefly, PTHPUDT was prepared by using the Grignard cross-coupling reaction according to the general method described by McCullough et al.[13] This polymer is regioregular, possessing a minimum 95% head-to-tail coupling, as determined by NMR spectroscopy. The weight-average molecular weight is 22 100 Daltons with a polydispersity (PDI) of 1.56.

Solutions of PTHPUDT were prepared by dissolving 5 mg of polymer in 5 mL of $CHCl_3$. Langmuir−Blodgett (LB) films were made by adding a known volume of polymer solution dropwise onto a fresh Millipore water subphase (18.2 MΩ-cm resistivity) onto a computer-controlled, Nima 600 series LB trough with a Wilhelmy plate pressure sensor. The LB barriers were compressed at a rate of 10 cm^2/min. Polymer films were deposited under pressure control at a surface pressure of 17.5 mN/m and at a dipping rate of 10 mm/min onto hydrophobic glass substrates. Glass substrates were made hydrophobic via the LB deposition of one monolayer of ferric stearate onto clean glass microscope slides at a surface pressure of 35 mN/m.

Mono- and multilayer films fabricated at variable temperatures employed an RM6 Lauda recirculating water bath attached to the trough to control the temperature of the water subphase. UV−Vis absorption spectra were obtained from a Cary 3E (Varian) spectrophotometer. Polarized light microscopy images were acquired using an Olympus BX60 microscope with crossed polarizers. Ellipsometry measurements were conducted with a Horiba Jobin Yvon UVISEL UV−Vis−NIR ex situ phase-modulated spectroscopic ellipsometer. Fluorescence measurements were conducted on polymer solutions, spin-cast, and LB-deposited films using a Photon Technology International (PTI) Quantamaster model QM1 and Ratiomaster model RC-M photomultiplier detection system. Atomic force microscopy (AFM) studies were carried out using a TM Microscopes Explorer scanning probe microscope system with an 8-μm *Z*-linearized dry scanner. AFM measurements were taken to assess the overall quality of the films and to determine film thickness. Film thickness measurements were obtained by scratching a portion of the film from the substrate and measuring the height of the unperturbed film in comparison to the region where the film had been removed.

Low-angle X-ray diffraction experiments were carried out using a RAPID (Rigaku) X-ray diffractometer with a copper target ($\lambda_{K\alpha} = 1.542$ Å) and an image plate detector. Transmission electron microscopy experiments were performed with an FEI Tecnai STEM 200 keV field emission STEM with a Lorentz lens and bi-prism, high angular annular dark field (HAADF) image filtering, energy dispersive (X-ray) spectroscopy (EDS), and a CCD detector. TEM studies were carried out on multilayer films deposited directly onto carbon-coated copper grids using the deposition conditions described above. Molecular modeling calculations were carried out with the program Molecular Modeling Basic revision 2.38 published by ChemSW Software, Inc.

Optical SHG measurements of PTHPUDT deposited onto a hydrophobic glass substrate were carried out using the regeneratively amplified output of a mode-locked titanium:sapphire oscillator. The detailed description of this optical set up has been previously reported.[14] Briefly, this system is capable of producing 100 fs pulses with energy of 1 mJ at a repetition rate of 1 kHz and nominal wavelength of 800 nm. Because pulses of such high peak intensity can lead to photochemical damage of the films under investigation, only a fraction (typically $<$50 mW) of the available laser power was employed during these studies. The polarization of the incident pulses was controlled by passing them through a quartz, zero-order, half-wave plate. The beam is then passed through an interference filter prior to striking the interface of interest in order to filter any second-harmonic light that may be generated at previously encountered mirror interfaces or in the quartz half-wave plate.

Film nonlinear susceptibility measurements were accomplished on LB-deposited PTHPUDT films using an external reflection geometry. External reflection measurements were

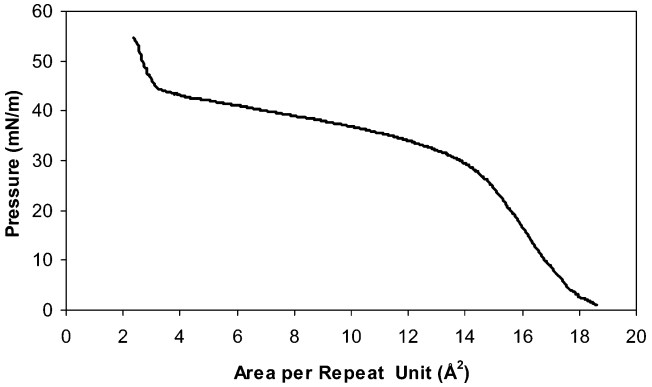

Figure 2. LB surface pressure vs area isotherm for PTHPUDT at room temperature.

made by monitoring the polarized SHG intensity from a 100-layer LB-deposited film as a function of the azimuthal rotation angle (ϕ) of the sample. Four polarization configurations corresponding to s- and p-polarized input and second-harmonic output beam polarizations were implemented. Experimental control was achieved by monitoring the SHG output from an isotropic film of malachite green (MG) prepared by spin-casting MG onto a similar substrate. Deposition of the multilayer films for the external reflection SHG studies was accomplished by standard dipping procedures onto microscope slides as described above.

Results and Discussion

Langmuir films of PTHPUDT were formed at the air/water interface of the LB trough by the addition of a 1.0 mg/mL solution of PTHPUDT in $CHCl_3$. The barriers of the trough were compressed and the resulting surface pressure-area ($\pi-A$) isotherms obtained at various temperatures were recorded. One such isotherm is displayed in Figure 2. The shape of the isotherms was very reproducible and subject to small changes with temperature. The isotherm in Figure 2 shows an initial increase in surface pressure at a molecular area (here considered as an area per repeat unit of the polymer) corresponding to approximately 20 Å^2. The surface pressure rises at a moderate rate with decreasing area until a surface pressure of approximately 30 mN/m is attained, at which point, the rate of increase in surface pressure with barrier compression decreases dramatically. This plateau region of the isotherm continues until a surface pressure ~43 mN/m is reached. Further barrier compression leads to a much faster rate of surface pressure increase until evidence of film collapse appears beyond surface pressures ~55 mN/m. Analysis of the first increase in surface pressure shows that the area per repeat unit when extrapolated to zero pressure corresponds to ~18 Å^2. Given that the tetrahydropyranyl moiety is hydrophilic, one might expect this zero-pressure area to be dictated by the THP functionality. Molecular modeling indicates that the THP moiety has a diameter of ~5.1 Å and that the zero-pressure area per repeat unit is consistent with the THP moiety being anchored into the water subphase and having some freedom to rotate. This area per repeat unit is consistent with a situation in which the plane of the polythiophene chain lies parallel to the water surface, with every pendant alkyl and THP group oriented toward the water subphase. Analysis of the second rise in surface pressure shows an area per repeat unit of ~7 Å^2 when extrapolated to zero pressure, roughly half of that corresponding to the first increase. It is possible that an increase in surface pressure from ~30 to ~43 mN/m leads to a change in the conformation of the polymer at the water surface with a transition to a polymer geometry in which the plane of the polymer backbone lies perpendicular (edge-on) to the water surface with every second THP group anchored into the subphase, consistent with a substantially smaller area per repeat unit. Indeed, as others have reported, variations of angle between the thiophene ring plane and the water surface are responsible for variations in the area per repeat unit of this magnitude.[7] Temperature-dependent studies of the isotherm behavior show that, as the temperature of the subphase is decreased, the area per repeat unit undergoes a small decrease as well, but the general shape of the isotherms remain unchanged.

Attempts to transfer monolayers in an organized fashion onto hydrophilic substrates met with limited success. Deposition (transfer) ratios for multilayer films showed inconsistent transfer. In contrast to our attempts to deposit onto *hydrophilic* substrates, monolayers of PTHPUDT were easily transferred in an organized fashion via the vertical dipping mechanism of the trough onto *hydrophobic* glass substrates. Deposition was monitored by two means. The first was by noting the advancing and receding water contact angles as the substrate was passed through the monolayer-covered water surface, and the second was by the creation of a pink/purple film onto the previously clear substrate. Monitoring the transfer ratios confirmed a Langmuir−Blodgett film of Y-type architecture. Deposition ratios for the PTHPUDT polymer multilayer films are similar to those with the well-defined *head-to-head* and *tail-to-tail* architectures of simple fatty acid multilayer films. The measured deposition ratios were 1.0 ± 0.1 and indicated deposition on both the up- and downstrokes, consistent with a Y-type film structure. To deposit Y-type architectures, one requires considerable hydrophobicity of the surface film on the downstroke (advancing water contact angles ~90° or greater) and a hydrophilic film (receding water contact angle $\ll$90°) for deposition on the upstroke. The observed deposition behavior is consistent with hydrophilic interactions between the THP groups and hydrophobic interactions between the alkyl chains and thiophene backbones in adjacent layers. Aqueous contact angle measurements support this view. Our measurements provide contact angles of 85° for multilayer films, where one expects the final layer deposited to expose a hydrophobic film. The LB deposition technique precludes direct measurement of the water contact angle with conventional methods of the surface for the upstroke. However, it can be estimated visually by viewing the meniscus formed at the substrate surface as the substrate is withdrawn from the water subphase. In this way, the receding aqueous contact angle is estimated to be ~35°. In addition, the water contact angles of spin-cast films (where the polymer is expected to have a different and broader distribution of orientations) is substantially lower (~70°) than that of the LB deposited films.

Further confirmation of efficient and ordered deposition was obtained by monitoring the optical absorbance of films of various thicknesses. The maximum absorption of each film was plotted against the number of transferred layers (Figure 3) and a linear correlation was found, consistent with the near-unity transfer ratios observed for both the up- and downstrokes.

In addition to the observation of a linear increase in film absorption with film thickness, anisotropic behavior was observed via polarized UV−vis absorption experiments. It was established that the absorption of the polymer film depended on the electric vector of the incident beam. A greater absorption

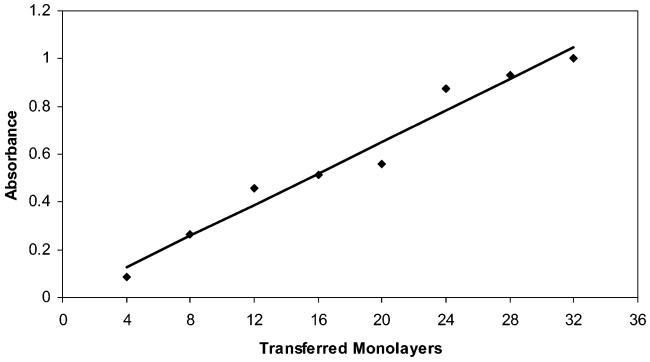

Figure 3. Absorbance vs number of transferred PTHPUDT layers.

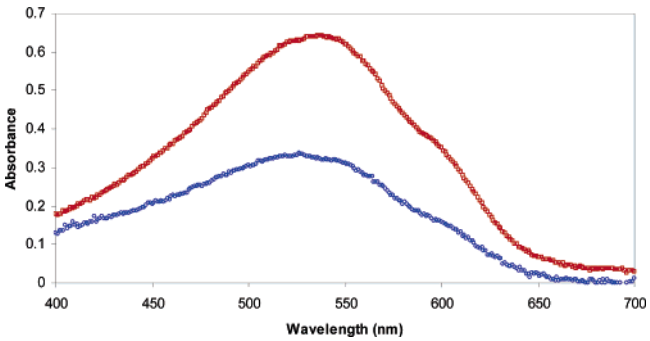

Figure 4. UV−vis absorption spectra for a 16-monolayer film of PTHPUDT: (1) electric vector parallel to the dipping direction (open squares); (2) electric vector orthogonal to the dipping direction (open circles).

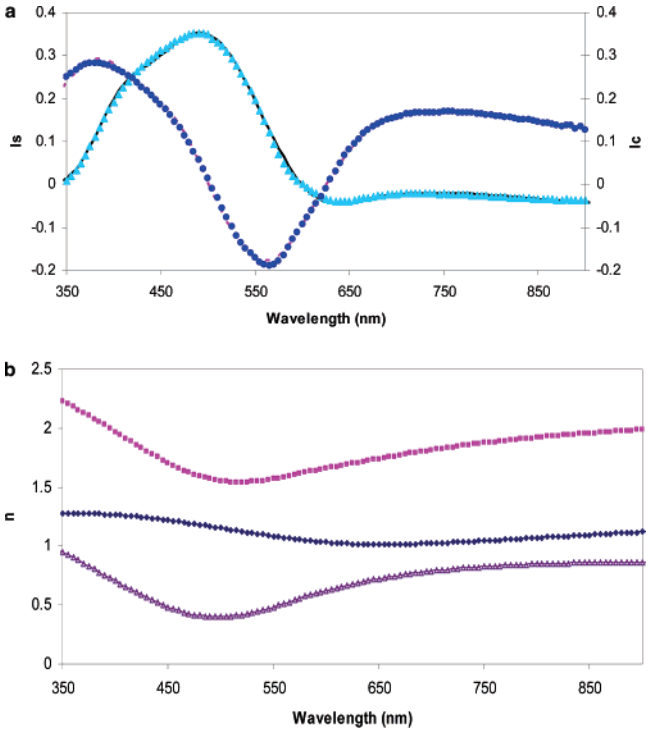

Figure 5. (a) Is (triangles) and Ic (circles) vs wavelength for a PTHPUDT LB film and their fits Is (solid line) and Ic (dashed line); (b) index of refraction as a function of wavelength along the ordinary (squares) and extraordinary axes (diamonds). The birefringence (triangles) is also plotted vs wavelength.

was found when the electric vector of the incident beam was parallel to the dipping direction rather than when it was perpendicular. Moreover, the absolute value of the absorbance was twice as large with the electric vector parallel to the dipping direction as compared to when perpendicular to the dipping direction (Figure 4). The maximum wavelength of absorption was also different in the two orientations: 550 nm with light polarized parallel to the dipping direction versus 525 nm with light polarized perpendicular to the dipping direction. This type of observation has been previously described[10,15,16] for highly oriented systems and is attributed to a change in conjugation length with orientation, meaning that longer chains are preferentially oriented along the dipping direction compared to shorter chains.

The anisotropic nature of the film was confirmed upon observing the films between crossed polarizers. No light was seen to pass through the system, and a dark field of view was present when the polarizer and analyzer were positioned at right angles to each other. However, with the addition of an 88-monolayer PTHPUDT film between the crossed polarizers, a uniform color (a measure of the optical retardation) was observed over the entire film. A $\lambda/4$ accessory plate was inserted into the optical path in order to improve the contrast. This resultant color change was subsequently interpreted with the help of a polarization color chart and was found to be first-order yellow. As the specimen was rotated relative to the polarizers, the intensity of the polarization color varied cyclically, from zero (extinction) up to a maximum after a 45° rotation and back down to zero after a 90° rotation.

The directions associated with the film birefringence were determined with the aid of the wave plate and found to be parallel/perpendicular to the LB dipping direction (high index parallel to the dipping direction.) Optical retardation values were measured at individual points throughout the film and then used to calculate the size of the birefringence at 23 °C and 550 nm. The birefringence was found to be of magnitude 0.56 and constant across the film.

Upon cooling the film to −180 °C followed by heating to 30 °C, the film was found to exhibit uniform birefringence of constant magnitude. However, when heated to 50 °C under a constant flow of N_2 gas, the film resulted in an irreversible extinction (dark) as the stage was rotated by 360°, indicating a loss of anisotropy. This behavior can be attributed to the loss of order in the film resulting from alkyl chain melting processes. Further studies are underway to help elucidate the detailed mechanism for loss of film order.

Ellipsometry measures the change in polarization state of light reflected from the surface of a film to provide information regarding film thickness and index of refraction. The measurable quantities in this experiment are related to the values of the variables Ψ and Δ as described in eqs 1−3 below and are plotted in Figure 5a. These variables are related to the ratio of Fresnel reflection coefficients, R_p and R_s for p- and s-polarized light and, therefore, to the refractive index.

$$\tan(\Psi)\, e^{i\Delta} = \frac{R_p}{R_s} \tag{1}$$

$$I_s = \sin 2\Psi \sin \Delta \tag{2}$$

$$I_c = \sin 2\Psi \cos \Delta \tag{3}$$

Figure 5a shows the ellipsometric data as well as the best fit to these data assuming a simple model for the film. The model consisted of a bottom layer assumed to be a layer of voids (if your substrate and or layer are assumed to be porous, void space

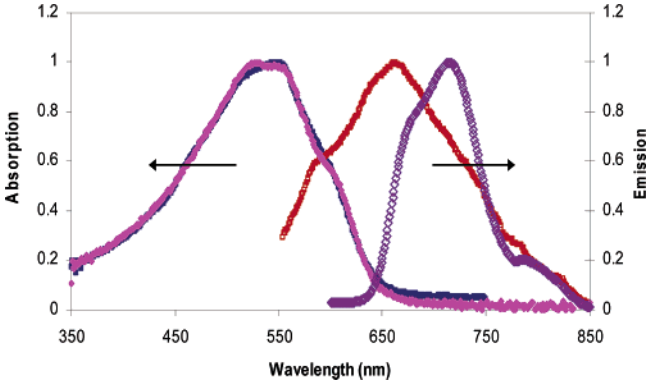

Figure 6. Solid-state absorption and emission spectra for spin-cast and LB films. Spin-cast absorption (closed diamonds), emission (open diamonds), LB absorption (closed squares), and emission (open squares).

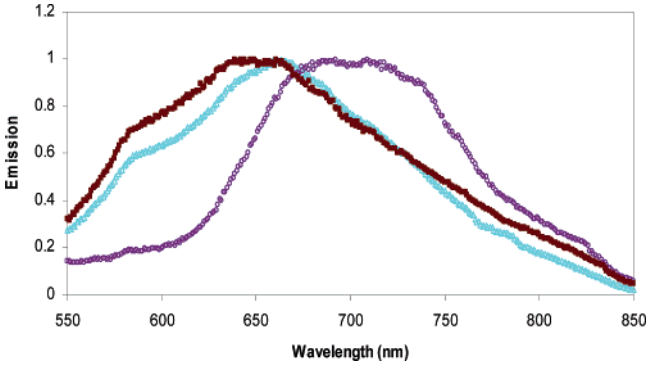

Figure 7. Polarized emission as a function of wavelength (a) without a polarizer (triangles), (b) with light polarized parallel to the dipping direction (open circles), (c) with light polarized perpendicular to the dipping direction (closed squares).

is treated like a chemical material.) Above this layer was placed a 1-mm-thick SiO_2 layer. The optical parameters associated with these layers were provided with the analysis software. To account for film birefringence, on top of the SiO_2 layer were placed two layers of PTHPUDT of equal thickness with different orthogonal indices of refraction. The total thickness of these two layers was a variable fitting parameter assumed to be 1320 Å, the thickness measured from an 88-monolayer PTHPUDT LB film via AFM. The ordinary and extraordinary refractive indices were allowed to vary independently and the fit optimized by standard least-squares methods.

To extract physical parameters of the sample such as optical constants, I_s and I_c were plotted versus the wavelength. Then an optical model describing the sample structure that accounted for all the layers in the sample was created. Theoretical data from the optical model that corresponded to the experimental data was generated. The generated data was then compared to the experimental data and the unknown parameters were varied to try and produce a "best fit" to the experimental data. Regression algorithms were used to vary the unknown parameters and minimize the difference between the generated and experimental data. The film thickness associated with the best fit was found to be 1133.807 ± 16.165 Å, which is reasonably close to the experimentally determined thickness of 1320 Å. The data are fitted very well over the entire spectral range by this simple model.

From this model, the index of refraction along both the ordinary and extraordinary axes and the resulting film birefringence were determined (Figure 5b). The value of the birefringence at 550 nm obtained from the ellipsometry measurements was found to be 0.48, in reasonable agreement with the value of 0.56, obtained from the white light source of the polarized light microscope. Examination of Figure 5b indicates that the film displays a large birefringence, particularly toward the ultraviolet spectral region. It should be noted that these birefringence data arise from an 88-layer film and, as such, represent a sizable optical retardation per molecular layer.

LB films of PTHPUDT were also found to be luminescent. The results of fluorescence studies carried out on spin-cast and LB-deposited films are presented in Figure 6. The excitation wavelength for the emission spectra of the spin-cast films was 520 nm, while that for the LB films was 550 nm. It should be noted that the wavelength of maximum absorption for the LB film is 30 nm red-shifted (550 nm) with respect to the spin-cast film (520 nm). The LB film emission maximum (666 nm) is blue-shifted ~50 nm with respect to the spin-cast film emission maximum (714 nm). The LB film shows two features, a shoulder at 591 nm and a peak at 666 nm. The spin-cast film exhibits three features, a shoulder at 679 nm and peaks at 714 and 790 nm. These features are attributed to a combination of Davydov splitting and the inherent excitonic band structure that results from aggregation of the polymer backbone.[17]

Fluorescence collected through a polarizer placed after the film shows a maximum wavelength of emission of 709 nm with vertically polarized light and 644 nm with horizontally polarized light (Figure 7). This compares with an emission maximum of 660 nm when no polarizer was present. Thus, our results indicate that the fluorescence maxima can be controlled over a range of ~65 nm by varying the polarization angle and, further, that the orientational anisotropy observed in these films is correlated with chains of substantially different conjugation length.

The magnitude of the fluorescence signals from both the spin-cast and LB-deposited films of PTHPUDT were relatively small compared to films of other materials of comparable thickness that have been examined. In particular, photon count rates of the PTHPUDT film luminescence were on the order of 1−2 orders of magnitude smaller than those from films of poly(9,9-dihexylfluorene-*alt*-2,2′-bithiophene (PFTT). Nevertheless, our results indicate that the LB-deposited films possess a substantial degree of conjugation, as indicated by the polarized absorption and luminescence red-shifts compared to spin-cast films, and that the luminescence of the LB-deposited films is highly polarized, consistent with a high degree of alignment of the polymer chains in the films.

The results of X-ray analysis of a 100-layer LB film of PTHPUDT are shown in Figure 8. The XRD pattern shows the existence of three peaks appearing at 2.95°, 5.87°, and 8.97°, respectively. These have been assigned to the first-, second-, and third-order peaks of the repeating interlayer spacing, respectively, and are indexed in Table 1. These peaks correspond to an interlayer spacing normal to the surface of the substrate. It is worth noting that much thicker annealed spin-cast films have shown up to sixth-order diffraction peaks, as well as peaks at 19.5° and 23°, due to chain crystallization and π-stacking, respectively.[12] Note that both chain crystallization and π-stacking peaks are absent in this LB film. Also, in contrast to spin-cast films of PTHPUDT, annealing the LB film at 50 °C under vacuum for 20 min leads to the reduction and disappearance of the second- and third-order diffraction

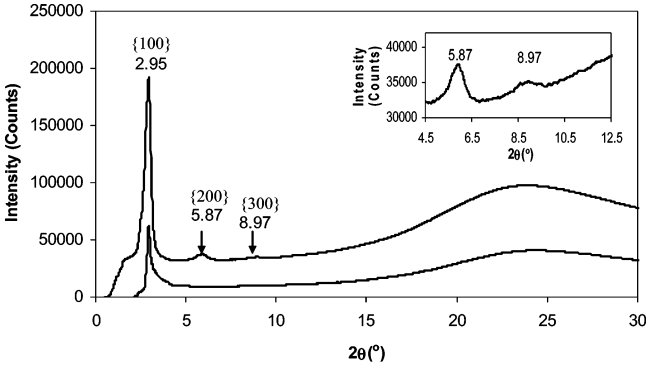

Figure 8. X-ray diffraction pattern from a 100-layer PTHPUDT LB film. Peak indexing of the film before heating (upper trace), and after heating at 50 °C for 20 min under vacuum (lower trace).

TABLE 1: Peak Indexing of the X-ray Diffraction Data Shown in Figure 8

2θ (deg)	$4 \sin^2 \theta/\lambda^2$	ratio	$h^2 + k^2 + l^2$	{}	d (Å)
2.95	0.0011	1.0	1	100	29.95
5.87	0.0044	4.0	4	200	15.06
8.97	0.0103	9.2	9	300	9.86

peaks, consistent with a loss of order in the film. Assuming an all-trans, fully extended side chain with adjacent thiophenes possessing coplanar conformations, the theoretical interlayer spacing is computed to be 42 Å.[12] This is considerably larger than the observed experimental interlayer spacing of 30 Å. Interdigitation of the tetrahydropyran-containing side chains would be unexpected due to the 5.1 Å diameter of the THP moiety. Rather, the *d* spacing is more likely a reflection of the bilayer repeat distance and is consistent with molecular modeling in which each thiophene unit has its THP-containing side chain oriented in the same direction, and the thiophene backbone remains planar and parallel to the substrate (Figure 9). Note that such a film structure would not be expected to give rise to a π-stacking diffraction peak because π-stacking would only occur between adjacent thiophene planes in each bilayer and no extended order at this length scale would develop. It is worth noting that previous work on regioregular, amphiphilic polythiophenes has shown *edge-on* conformation of the thiophene chains with respect to the surface. However, these studies have been focused on bithiophene-based polymers with a hydrophilic and hydrophobic pendant group on each thiophene subunit. Under these circumstances, it is not altogether surprising that films such as these would yield edge-on architectures. Edge-on architectures in the case of PTHPUDT, however, would provide hydrophilic THP moieties oriented both toward and away from the water surface. Such an orientation of the polymer chain would tend to preclude deposition in the "head-to-head and tail-to-tail" (HHTT) fashion, which produces the Y-type LB film structure observed here.

Atomic force microscopy (AFM) studies were conducted on a 38-monolayer thick film of PTHPUDT, LB-deposited onto a hydrophobic glass microscope slide. A portion of the film was scratched away in order to measure the thickness of the deposited film. The difference in height between the regions where the film remained undisturbed and where the film had been removed was 56.6 ± 0.2 nm. The expected thickness of the film (assuming a bilayer spacing of 30 Å and one monolayer of ferric stearate assumed to be 2.4 nm thick) was 59.4 nm, consistent with the measured value.

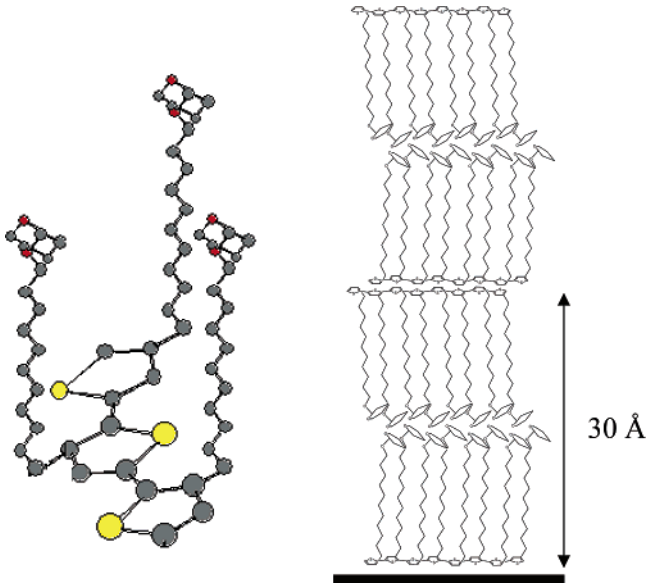

Figure 9. Orientation of PTHPUDT on a hydrophobic substrate. According to molecular modeling calculations, the interlayer distance is 31.6 Å.

Optical second-harmonic generation (SHG) can be used as a tool to investigate surface and interface structure,[18−21] providing information regarding adsorbate orientation.[22,23] This technique takes advantage of the inherently asymmetric environment of the interface formed between two bulk phases of matter. When the two bulk phases are both centrosymmetric, the noncentrosymmetric interface between them possesses a second-order nonlinearity ($\chi_s^{(2)}$), which can give rise to interface-specific, second-order, nonlinear optical effects. An intense laser beam of frequency ω and polarization $\hat{e}_\omega$ incident on a surface or interface at an angle ψ with respect to the surface normal will produce second-harmonic light at frequency 2ω and polarization $\hat{e}_{2\omega}$ with an intensity given by[21]

$$I_{2\omega} = \frac{32\pi^3}{c^3}(\omega^2)s^2\psi|\hat{e}_{2\omega}\cdot\chi_s^{(2)}(2\omega):\hat{e}_\omega\hat{e}_\omega|^2 I_\omega^2 \qquad (4)$$

In situations where the macroscopic second-order surface nonlinear susceptibility $\chi_s^{(2)}$ is large due to the presence of adsorbed molecules, contributions from the substrate and local field effects can be ignored and the susceptibility written as an averaged sum of the second-order nonlinear molecular polarizabilities ($\beta^{(2)}$) of the adsorbed species

$$\chi_s^{(2)} = N_s\langle\beta^{(2)}\rangle \qquad (5)$$

where N_s is the number of adsorbate molecules on the surface and the brackets denote an average taken over all adsorbate orientations. Thus, given information regarding the molecular polarizabilities, measurement of the surface susceptibility can provide an indication of the averaged molecular orientation. The polarization dependence of the surface second-harmonic response can be used to extract the elements of the second-order nonlinear susceptibility tensor $\chi^{(2)}$ and, therefore, used to obtain orientation information. The sample is assumed to be anisotropic, possessing C_{1v} symmetry. Under these conditions, the polarization dependence of the sample can be related to the 10 nonzero tensor elements of $\chi_s^{(2)}$ by eq 6.[24,25]

s-in−s-out

$$\chi_{\mathrm{eff}}^{(2)} = -\chi_{xxx}^{(2)}(\sin^3\phi)L_y(2\omega)L_y^2(\omega) - 2\chi_{yyx}^{(2)}(\cos^2\phi)(\sin\phi)L_y(2\omega)L_y^2(\omega) - \chi_{xyy}^{(2)}(\cos^2\phi)(\sin\phi)L_y(2\omega)L_y^2(\omega)$$

p-in−s-out

$$\chi_{\mathrm{eff}}^{(2)} = -\chi_{xxx}^{(2)}(\cos^2\phi)(\sin\phi)L_y(2\omega)L_x^2(\omega)\cos^2\theta_1(\omega) + 2\chi_{yyx}^{(2)}(\cos^2\phi)(\sin\phi)L_y(2\omega)L_x^2(\omega)\cos^2\theta_1(\omega) - \chi_{xyy}^{(2)}(\sin^3\phi)L_y(2\omega)L_x^2(\omega)\cos^2\theta_1(\omega) - 2(\chi_{xxz}^{(2)} - \chi_{yyz}^{(2)})(\sin\phi)(\cos\phi)L_y(2\omega)L_x(\omega)L_z(\omega)[-\sin\theta_1(\omega)\cos\theta_1(\omega)] - \chi_{xzz}^{(2)}(\sin\phi)L_y(2\omega)L_z^2(\omega)\sin^2\theta_1(\omega)$$

s-in−p-out

$$\chi_{\mathrm{eff}}^{(2)} = \chi_{xyy}^{(2)}(\cos^3\phi)L_x(2\omega)L_y^2(\omega)\cos\theta_1(2\omega) + \chi_{xxx}^{(2)}(\sin^2\phi)(\cos\phi)L_x(2\omega)L_y^2(\omega)\cos\theta_1(2\omega) - 2\chi_{yyx}^{(2)}(\sin^2\phi)(\cos\phi)L_x(2\omega)L_y^2(\omega)\cos\theta_1(2\omega) + \chi_{zxx}^{(2)}(\sin^2\phi)L_z(2\omega)L_y^2(\omega)\sin\theta_1(2\omega) + \chi_{zyy}^{(2)}(\cos^2\phi)L_z(2\omega)L_y^2(\omega)\sin\theta_1(2\omega)$$

p-in−p-out

$$\chi_{\mathrm{eff}}^{(2)} = \chi_{xxx}^{(2)}(\cos^3\phi)L_x(2\omega)L_x^2(\omega)\cos\theta_1(2\omega)\cos^2\theta_1(\omega) + 2\chi_{yyx}^{(2)}(\sin^2\phi)(\cos\phi)L_x(2\omega)L_x^2(\omega)\cos\theta_1(2\omega)\cos^2\theta_1(\omega) + \chi_{xyy}^{(2)}(\sin^2\phi)(\cos\phi)L_x(2\omega)L_x^2(\omega)\cos\theta_1(2\omega)\cos^2\theta_1(\omega) + \chi_{zxx}^{(2)}(\cos^2\phi)L_z(2\omega)L_x^2(\omega)\sin\theta_1(2\omega)\cos^2\theta_1(\omega) + 2\chi_{xxz}(\cos^2\phi)L_x(2\omega)L_x(\omega)L_z(\omega)[-\cos\theta_1(2\omega)\cos\theta_1(\omega)\sin\theta_1(\omega)] + \chi_{zyy}(\sin^2\phi)L_z(2\omega)L_x^2(\omega)\sin\theta_1(2\omega)\cos^2\theta_1(\omega) + 2\chi_{yyz}(\sin^2\phi)L_x(2\omega)L_x(\omega)L_z(\omega)[-\cos\theta_1(2\omega)\cos\theta_1(\omega)\sin\theta_1(\omega)] + \chi_{xzz}^{(2)}(\cos\phi)L_x(2\omega)L_z^2(\omega)\cos\theta_1(2\omega)\sin^2\theta_1(\omega) + 2\chi_{zxz}^{(2)}(\cos\phi)L_z(2\omega)L_x(\omega)L_z(\omega)[-\sin\theta_1(2\omega)\sin\theta_1(\omega)\cos\theta_1(\omega)] + \chi_{zzz}^{(2)}L_z(2\omega)L_z^2(\omega)\sin\theta_1(2\omega)\sin^2\theta_1(\omega) \quad (6)$$

The constants $L_i(\omega_j)$ in eq 6 are the Fresnel factors at the corresponding frequencies. The calculation of these constants has been outlined for a variety of different experimental geometries,[26,27] including that of external reflection, the geometry employed for these studies. The azimuthal angle ϕ is the angle between the plane of incidence and the angle of the C_{1v} axis, while the angle θ_1 is the angle of incidence of the laser beam with respect to the surface normal. By rotating the azimuthal angle of the sample under various polarization conditions, one can extract the individual tensor elements of $\chi_s^{(2)}$. Once obtained, these values of the macroscopic surface nonlinear susceptibility tensor can be related to the elements of the molecular nonlinear polarizibility tensor, β_{ijk}, to obtain the molecular orientation distribution function. The direction cosines required to evaluate the distribution function can be obtained from the Euler transformation connecting the molecular ($x'y'z'$) and laboratory (xyz) reference frames.

Figure 10 shows the polarized second-harmonic generation signals from a 100-layer LB film of PTHPUDT and their corresponding best fits to the experimental data assuming a functional dependence as described in eq 6. In this experiment, the SH intensity was monitored as a function of the azimuthal orientation angle of the sample, ϕ, for different input and detected output polarization geometries. Also shown in Figure 10 are the data and best fit curves for an isotropic film of malachite green (MG). As expected for an isotropic film, the SH data from MG is isotropic in ϕ. SHG with s-in−s-out and p-in−s-out geometries is symmetry forbidden in an isotropic film and, therefore, generated no detectable signal. It is clear from Figure 10 that SHG from the 100-layer polymer LB film is indeed anisotropic. This is supported by the clear anisotropic nature of the signal as well as the nonzero signal level obtained in the s-in−s-out geometry. The best fits were determined by a nonlinear least-squares fitting algorithm, which permitted the extraction of the individual nonvanishing components of the $\chi^{(2)}$ tensor.

The s-in−s-out SH signal was fitted first to obtain the best fit values of the three elements describing its functional dependence, as described in eq 6. These elements were then held fixed for the fitting of the p-in−s-out curves and so on until all polarization curves had been fitted in succession. The elements of $\chi^{(2)}$ so determined are presented in Table 2.

As eq 5 indicates, a complete description of the orientation distribution function also depends on which components of the nonlinear polarizability tensor contribute to the total molecular polarizability. This calculation can be simplified for many molecules by assuming that only one element of the polarizability tensor contributes significantly to the molecular nonlinear response in the UV−visible spectral region. β is a tensor that is formed by the direct product of the vectors r_{ng} (transition dipole matrix element between the excited-state n, and the ground-state g along the molecular x' axis) and Δr_n (the difference in permanent dipole moment between n and g).[21] In the case of polythiophenes, the optical properties are governed primarily by the π electrons in the thiophene backbone and display only one dominant low-energy excited electronic state. The corresponding transition dipole for the $S_1 \leftarrow S_0$ transition is polarized along the z' molecular axis and is responsible for the strong absorption of polythiophenes in the vicinity of 400 nm.

Unsubstituted polythiophene is centrosymmetric, and one expects no second-order nonlinear response from it unless its polarization is distorted. Substituents added to the polythiophene chain may break this center of symmetry; however, to a first order of approximation, one expects, at best, weak second-order nonlinear response. As illustrated in Figure 1, regioregular PTHPUDT is noncentrosymmetric due to the net orientation of its pendant chains, but as noted, second-harmonic signals from PTHPUDT films are very small. What level of second-order response there is, is likely due to the highly ordered and anisotropic alignment of molecules in the film, in conjunction with the low-energy z' polarized transition in near two-photon

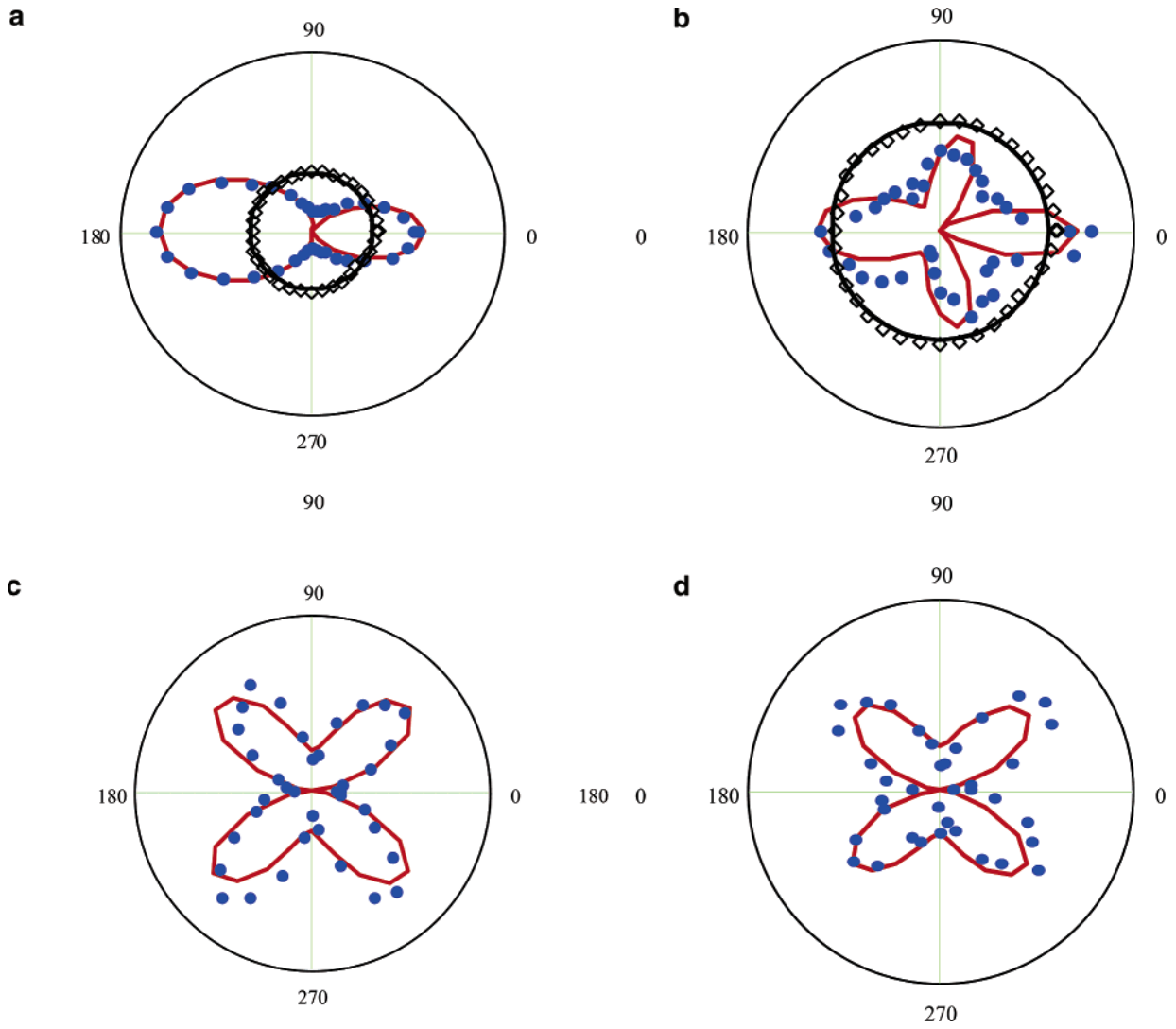

Figure 10. Polarized second-harmonic intensity vs azimuthal angle for an LB film with 100 monolayers of PTHPUDT deposited onto one monolayer of ferric stearate on a hydrophilic glass slide. The input−output polarization combinations are: (a) p-in−p-out, (b) s-in−p-out, (c) s-in−s-out, (d) p-in−s-out. The points represent the collected data. The solid lines represent a nonlinear least-squares best fit to the data. The open diamonds represent data for an isotropic malachite green film spin-cast onto a glass slide. The dipping direction corresponds to 90°.

TABLE 2: Relative Susceptibility Components Used to Fit Experimentally Determined SHG Data from Figure 10

χ_{zzz}	=	−0.01
χ_{zxx}	=	−3.92
χ_{zyy}	=	0.15
χ_{xxx}	=	1.31
χ_{xzz}	=	11.29
χ_{yyx}	=	1.40
χ_{xyy}	=	2.40
χ_{yyz}	=	−2.42
χ_{xxz}	=	−2.40
χ_{xzz}	=	−14.00

resonance with our fundamental frequency. Because r_{ng} and Δr_n are collinear for the case of PTHPUDT, it may be reasonable to expect that only the β_{zzz} term contributes significantly to the observed nonlinear response.

By evaluating the product of direction cosines implied by eq 5, and assuming that β_{zzz} is the only dominant component of the hyperpolarizability, one can derive a relationship describing the averaged orientation within the film.[28] Equation 7 describes the molecular orientation parameter D ($= \langle \cos^2 \theta \rangle$, where θ is the tilt angle of the molecular z' axis relative to the surface normal, z), expressed in terms of the experimentally determined susceptibility components:

$$D = \frac{\chi_{zzz}}{\chi_{zzz} + \chi_{zxx} + \chi_{zyy}} \tag{7}$$

Under these circumstances, eq 7 dictates that the angle θ between the surface normal and the molecular z' axis is ~90° ± 5°. This is consistent with an orientation in which the thiophene backbone lies parallel to the surface. This orientation correlates well with the thickness and order of the films we have previously measured. However, it should be recognized that, with the assumption of β_{zzz} as the only dominant component of the hyperpolarizability tensor, one also expects a simplification in eq 6 and a reduction in the number of independent susceptibility elements from 10 to 6.[28] Our attempts to model the data with such a restriction do not allow a satisfactory set of fits to the experimental data of Figure 10. The inability to obtain adequate fits in the limit of this restriction calls into question the assumption of a single contributing element of the hyperpolarizability tensor.

In general, the agreement between the experimental and fitted data presented in Figure 10 is good. However, small differences

between the fit and data are apparent in Figure 10b (the s-in−p-out curve). In an attempt to improve the fit for this curve, all of the parameters associated with it were allowed to vary. The fit improved slightly; however, the parameters required for this yielded fits of slightly lower quality for Figure 10a and d. The angle obtained using these parameters was similar to that obtained by our original fitting procedure and used to provide a measure of the uncertainty in the averaged orientation angle extracted from the fits.

It should also be noted that, in this analysis, we have ignored some important aspects of the local field effects. In particular, while we have compelling evidence for film birefringence, we have not formally incorporated this in-plane birefringence into our fitting algorithm. While the importance of accounting for the effects of birefringence in SHG analyses in uniaxial systems has been recognized,[29] the effects of in-plane birefringence have not yet been appropriately addressed. We are currently attempting to incorporate these effects into our model, and the results will be presented in a forthcoming publication.

Knowledge of the interfacial optical constants is critical for relating the macroscopic SHG polarization measurements to the $\chi^{(2)}$ tensor elements describing the nonlinear optical response of the interface. Even subtle differences in the assumed optical constants for the nonlinear optically active interfacial layer can produce substantial changes in the calculated $\chi^{(2)}$ tensor elements describing the surface and, correspondingly, in the interpretation of surface structure.[30] One approach to evaluate the linear interfacial optical constants is simply to assign the interfacial refractive index to be identically equal to one of the two media at the interface.[26,28,31,32] However, it is not clear which of the two media should be selected and why one should be preferred over the other. Others have employed models in which the refractive index is intermediate between the two bulk interfacial media.[33−36] The results obtained using these approaches appear to be generally quantitatively reliable. In this regard, there are two possible limiting cases.

For the case where the film thickness is far less than the wavelength of light, the effective refractive index for the interfacial layer becomes the average of the two media sandwiching the interface. We find ourselves in the case where film thickness is on the order of the wavelength of light. In this case, the effective refractive index for the interfacial layer is simply the average refractive index within the multilayer film, recovering expressions similar to those currently used widely to interpret polarization phenomena in SHG surface measurements.[29] For the purposes of the current work, our simplified analysis is sufficient to capture the nature of the anisotropy in the film and provide a reasonable estimate of the averaged polymer orientation within the film. Nevertheless, an appropriate mechanism for dealing with the experimentally observed in-plane birefringence is needed in order to extract more meaningful orientation information from the data.

Conclusions

Taken together, our data suggest that LB films constructed from PTHPUDT form highly ordered multilayer structures. Layer-by-layer deposition affords Y-type architectures that possess considerable in-plane anisotropy, as demonstrated by anisotropic optical absorption, emission, and direct birefringence measurements. These films are of optical quality and possess uniform optical retardation over the film. Our data suggest that the polymer's thiophene backbone lies parallel to the surface, with its pendant alkyl groups oriented normal to the surface in such a way as to form an amphiphilic structure. These films offer a unique opportunity to examine both the thermal chemistry and photochemistry of deprotection in highly ordered environments and suggest a route for the construction of highly ordered polymers with optimized luminescent or conducting properties. We are currently investigating the effects of film order on the rates and mechanisms of the thermal and photochemical deprotection characteristic of these polymer systems.

Acknowledgment. We thank the Natural Sciences and Engineering Research Council of Canada and Simon Fraser University for financial support. We also thank Professor Hogan Yu for the use of his contact angle instrument and Professor Z-G. Ye for use of his polarized light microscope.

References and Notes

(1) Fairley, P. *Chem. Week*, June 3, 1998; p 42.

(2) Sirringhaus, H.; Tessler, N.; Friend, R. H. *Science* **1998**, *280*, 1741−1744.

(3) Xu, B.; Holdcroft, S. *Macromolecules* **1993**, *26*, 4457−4460. (b) Chen, T.; Wu, X.; Rieke, R. D. *J. Am. Chem. Soc.* **1995**, *117*, 233−244. (c) McCullough, R. D.; Lowe, R. D. *J. Chem. Soc., Chem. Commun.* **1992**, 70−72.

(4) (a) *Handbook of Organic Conductive Molecules and Polymers*: *Conducting Polymers: Transport, Photophysics and Applications*; Nalwa, H. S., Ed.; John Wiley & Sons: New York, 1997; Vol. 4. (b) Chen, T.; Rieke, R. D. *Synth. Met.* **1993**, *60*, 175−177. (c) Greenham, N. C.; Friend, R. H. In *Physical Properties of Polymers Handbook*; Mark, J. E., Ed.; AIP Press: Woodbury, NY, 1996; pp 479−487.

(5) Sirringhaus, H.; Brown, P. J.; Friend, R. H.; Nielsen, M. M.; Bechgaard, K.; Langeveld-Voss, B. M. W.; Spiering, A. J. H.; Janssen, R. A. J.; Meijer, E. W.; Herwig, P.; de Leeuw, D. M. *Nature* **1999**, *401*, 685−688.

(6) Kim. J.; Swager, T. M. *Nature* **2001**, *411*, 1030−1034.

(7) Callender, C. L.; Carere, C. A.; Daoust, G.; Leclerc, M. *Thin Solid Films* **1991**, *204*, 451−457.

(8) Sagisaka, S.; Ando, M.; Iyoda, T.; Shimidzu, T. *Thin Solid Films* **1993**, *230*, 65−69.

(9) Bolognesi, A.; Bajo, G.; Geng, Z.; Porzio, W.; Speroni, F. *Thin Solid Films* **1994**, *243*, 683−686.

(10) Bolognesi, A.; Bertini, F.; Bajo, G.; Provasoli, A.; Villa, D.; Ahumada, O. *Thin Solid Films* **1996**, *289*, 129−132.

(11) Reitzel, N.; Greve, D. R.; Kjaer, K.; Howes, P. B.; Jayaraman, M.; Savoy, S.; McCullough, R. D.; McDevitt, J. T.; Bjornholm, T. *J. Am. Chem. Soc.* **2000**, *122*, 5788−5800.

(12) Yu, J.; Holdcroft, S. *Chem. Mater.* **2002**, *14*, 3705−3714.

(13) McCullough, R. D.; Lowe, R. D.; Jayaraman, M.; Anderson, D. L. *J. Org. Chem.* **1993**, *58*, 904−912.

(14) Kikteva, T.; Star, D.; Zhao, Z.; Baisley, T. L.; Leach, G. W. *J. Phys. Chem. B* **1999**, *103*, 1124−1133.

(15) Wu, A.; Akagi, T.; Jikei, M.; Kakimoto, M.; Imai, Y. *Thin Solid Films* **1996**, *273*, 214−217.

(16) Danno, T.; Kurti, J.; Kuzmany, H. *Phys. Rev. B* **1991**, *43*, 4809−4819.

(17) Vamvounis, G.; Yu, J.; Holdcroft, S. *Eur. Polym. J.* **2004**, *40*, 2659−2664.

(18) Shen, Y. R. *Annu. Rev. Phys. Chem.* **1989**, *40*, 327−350; *Nature* **1989**, *337*, 519−525.

(19) Richmond, G. L.; Robinson, J. M.; Shannon, V. L. *Prog. Surf. Sci.* **1988**, *28*, 1−70.

(20) Eisenthal, K. B. *Annu. Rev. Phys. Chem.* **1992**, *43*, 627−661.

(21) Corn, R. M.; Higgins, D. A. In *Characterization of Organic Thin Films*; Ulman, A., Ed.; Butterworth-Heinemann: Boston, MA, 1995; pp 227−247.

(22) Higgins, D. A.; Byerly, S. K.; Abrams, M. B.; Corn, R. M. *J. Phys. Chem.* **1991**, *95*, 6984−6990.

(23) Higgins, D. A.; Abrams, M. B.; Byerly, S. K.; Corn, R. M. *Langmuir* **1992**, *8*, 1994−2000.

(24) Bloembergen, N.; Pershan, P. S. *Phys. Rev.* **1962**, *128*, 606−622.

(25) Hirose, C.; Akamatsu, N.; Domen, K. *Appl. Spectrosc.* **1992**, *46*, 1051−1072.

(26) Mizrahi, V.; Sipe, J. E. *J. Opt. Soc. Am. B* **1988**, *5*, 660−667.

(27) Felderhof, B. U.; Bratz, A.; Marowsky, G.; Roders, O.; Sieverdes, F. *J. Opt. Soc. Am. B* **1993**, *10*, 1824−1833.

(28) Feller, M. B.; Chen, W.; Shen, Y. R. *Phys. Rev. A* **1991**, *43*, 6778−6792.

(29) Roy, D. *Phys. Rev. B* **2000**, *61*, 13283−13286.

(30) Simpson, G. J.; Dailey, C. A.; Plocinik, R. M.; Moad, A. J.; Polizzi, M. A.; Everly, R. M. *Anal. Chem*. **2005**, *77*, 215−224.
(31) Heinz, T. F.; Tom, H. W. K.; Shen, Y. R. *Phys. Rev. A* **1983**, *28*, 1883.
(32) Heinz, T. F.; Chen, C. K.; Ricard, D.; Shen, Y. R. *Phys. Rev. Lett.* **1982**, *48*, 478−481.
(33) Ekhoff, J. A.; Rowlen, K. L. *Anal. Chem.* **2002**, *74*, 5954−5959.
(34) Fordyce, A. J.; Bullock, W. J.; Timson, A. J.; Haslam, S.; Spencer-Smith, R. D.; Alexander, A.; Frey, J. G. *Mol. Phys.* **2001**, *99*, 677−687.
(35) Grudzkov, Y. A.; Parmon, V. N. *J. Chem. Soc., Faraday Trans*. **1993**, *89*, 4017−4026.
(36) Simpson, G. J.; Westerbuhr, S.; Rowlen, K. L. *Anal. Chem.* **2000**, *72*, 887−898.